AIMS Mathematics, 10(8): 19217–19239.
DOI: 10.3934/math.2025859
Received: 12 June 2025
Revised: 06 August 2025
Accepted: 20 August 2025
Published: 25 August 2025

https://www.aimspress.com/journal/Math

Research article

A new robust control framework for heat transfer equations through L_1 robust stability analysis and the design of a 2-DoF robust LQI controller

Taewan Kim[1], **Jung Hoon Kim**[1,*] **and Jihyun Park**[1,2]

[1] Department of Electrical Engineering, Pohang University of Science and Technology (POSTECH), Pohang 37673, Republic of Korea

[2] Smart Mobility R&D Division, Korea Institute of Robotics & Technology Convergence (KIRO), Pohang 37666, Republic of Korea

* **Correspondence:** Email: junghoonkim@postech.ac.kr; Tel: +82542792230; Fax: +82542792903.

Abstract: This paper developed a new robust control framework for uncertain heat transfer systems with a rapid thermal annealing (RTA) processes. We first employed the spatial discretization and Taylor linearization schemes in the nonlinear partial differential equation describing the dynamic behavior of heat transfer systems, by which a linear time-invariant (LTI) system with model uncertainties was derived. More precisely, the model uncertainties were decomposed into feedforward and feedback components, and they were shown to be bounded in terms of the L_∞(-induced) norm. This representation allowed us to establish an L_1 robust stability condition for uncertain heat transfer systems. We next designed a 2-degree-of-freedom (2-DoF) robust linear quadratic integral (LQI) controller to achieve the L_1 robust stability condition and reduce the effects of the model uncertainties on the associated tracking accuracy. Finally, some simulations were given to verify the effectiveness of the developed method.

Keywords: heat transfer equations; L_1 robust stability; 2-DoF control; small-gain theorem
Mathematics Subject Classification: 93D09

1. Introduction

Precise temperature control in distributed thermal systems is crucial for ensuring uniformity and reliability in applications such as the semiconductor manufacturing [1, 2] and the microelectronic packaging [3]. They are described by nonlinear heat transfer equations, typically expressed as partial differential equations (PDEs). To proceed a controller synthesis in an efficient form, spatial discretization techniques such as the finite-difference method [4] and the finite-element method [5] are employed for converting these PDEs into finite-dimensional ordinary differential equations (ODEs).

An extensive discussion of these discretization techniques is provided in [6]. Even though various results on such approximations are introduced in [7,8], they intrinsically derive modeling errors, which could adversely affect the associated stability/performance.

The effects of the aforementioned modeling errors on the tracking accuracy for heat transfer systems are considered in [9, 10] by developing some arguments on proportional-integral-derivative (PID) control and linear quadratic regulator (LQR), respectively, but no assertion on ensuring a robust stability of heat transfer systems in the presence of uncertain elements is provided in those studies. In this line, an observer-based strategy is proposed in [11] to estimate the modeling errors and compensate their effects on the associated stability/performance for heat transfer systems. However, the assertions in [11] are confined to time-invariant uncertainties, and thus applying the results in that study to heat transfer systems might be vulnerable to the case of time-varying uncertainties.

To address this issue, we are concerned with establishing a new control framework for heat transfer systems with both time-invariant and time-varying modeling errors. To this end, we introduce a new description of nonlinear heat transfer systems with norm-bounded model uncertainties. Motivated by the fact that model uncertainties occurring from spatial discretizations are generally described by constants and/or slowly varying biases, we take the L_∞ norm and its induced norm to evaluate such uncertainties. Here, the L_∞ is taken as an underlying space for a wide class of systems such as discrete-time systems [12], Euler-Lagrange systems [13, 14], nonlinear piecewise continuous systems [15], and hybrid continuous/discrete-time systems [16], but no discussion on taking the L_∞ space for nonlinear heat transfer systems is provided in the literature. To put it another way, this paper establishes an L_1 robust stability condition for heat transfer systems with model uncertainties characterized by the L_∞(-induced) norm for the first time; the problem of dealing with the L_∞ norm has been called the L_1 problem as in [16, 17]. The L_1 robust stability condition is constructed based on a new description of nonlinear heat transfer systems as an interconnection between a nominal linear system and a nonlinear model uncertainty bounded by the L_∞-induced norm, and this allows us to ensure that nonlinear heat transfer systems are robustly stable. For a high accuracy of a rapid thermal annealing (RTA) process of heat transfer systems, we also design a 2-degree-of-freedom (2-DoF) robust linear quadratic integral (LQI) controller, by which the effects of the model uncertainty on the associated reference tracking accuracy can be reduced and the zero steady-state tracking error is achieved. To summarize, the main contributions of this paper over the conventional studies [9–11] can be described as follows.

- A new description of nonlinear heat transfer systems with time-invariant and time-varying uncertainties as an interconnection of a linear nominal system and a model uncertainty bounded by the L_∞(-induced) norm.
- A robust stability condition for uncertain nonlinear heat transfer systems in terms of the L_∞-induced norm, i.e., the L_1 robust stability condition.
- High tracking accuracy through a 2-DoF robust LQI controller design for uncertain nonlinear heat transfer systems.

The remainder of this paper is organized as follows. The description of heat transfer systems and their spatial discretization procedure are introduced in Section 2. The main results of this paper, i.e., the interconnected representation, the L_1 robust stability condition, and the 2-DoF robust LQI control framework, are derived in Section 3. Some comparative simulations and the relevant discussions are given in Section 4. Concluding remarks are provided in Section 5. Finally, the notations used in this paper are summarized in Table 1.

Table 1. The notations used in this paper.

Notation	Meaning
$\mathbb{R}^p$	The set of p-dimensional real vectors
1_n	The n-dimensional whose every element is one, i.e., $1_n := \begin{bmatrix} 1 & 1 & \cdots & 1 \end{bmatrix}^T \in \mathbb{R}^n$
I_n	The $n \times n$-dimensional identity matrix
$\lvert\cdot\rvert_\infty$	The ∞-norm of a real vector or a matrix, i.e., $\lvert v\rvert_\infty := \max_i \lvert v_i\rvert$ or $\lvert A\rvert_\infty := \max_i \sum_j \lvert a_{ij}\rvert$
$\lVert\cdot\rVert_\infty$	The L_∞-norm of a vector function, i.e., $\lVert f(\cdot)\rVert_\infty := \operatorname{ess\,sup}_{0\le t<\infty} \lvert f(t)\rvert_\infty$
diag$(\cdot)$	Diagonal matrix formed from its augments
$Q \succ 0$	A symmetric matrix Q is positive definite, i.e., $x^T Qx > 0$, $\forall x(\neq 0) \in \mathbb{R}^n$
$\times_i$	Tensor-matrix product along the i-th dimension

2. Description of heat transfer processes

This section first reviews a method for describing heat transfer processes [11], in which a uniform temperature distribution is considered when some lamps are installed to apply heat to a wafer. More precisely, let us consider the wafer as shown in Figure 1, whose heat transfer process can be described by the one-dimensional partial differential equation PDE*

$$\frac{\partial T(r,t)}{\partial t} = \kappa(T)\left[\frac{\partial^2 T(r,t)}{\partial r^2} + \frac{1}{r}\frac{\partial T(r,t)}{\partial r}\right], \tag{2.1}$$

where r is the radial distance, t is the time, $T(r,t)$ is the temperature, and $\kappa(T) = \lambda_c(T)/(\rho c_p(T))$ with the heat conductivity $\lambda_c(T)$, the heat capacity $c_p(T)$, and the density ρ of the wafer. Because it is quite difficult to obtain meaningful arguments for dealing with a heat transfer process of the wafer by using (2.1) itself, the so-called central difference approximation as shown in Figure 2 is introduced [11]. To put it another way, the left-hand side (LHS) of (2.1) is approximated in [11] by

$$\frac{\partial T(r,t)}{\partial r} \approx \frac{T(r+\delta_r,t) - T(r-\delta_r,t)}{2\delta_r}, \tag{2.2}$$

where $\delta_r = R/n$, R is the radius of the wafer, and n is the approximation parameter (i.e., the number of rings in Figure 2). In an equivalent fashion, we can also obtain the approximation given by

$$\frac{\partial^2 T(r,t)}{\partial r^2} \approx \frac{T(r+\delta_r,t) - 2T(r,t) + T(r-\delta_r,t)}{\delta_r^2}. \tag{2.3}$$

For $i = 1,\ldots,n$, let us further define $T_i := T(r_i,t)$ with $r_i = \chi_i\delta_r$ and $\chi_i = (2i-1)/2$. Then, substituting (2.2) and (2.3) into (2.1) at $t = t_i$ leads to the n-coupled ODEs described by

$$\frac{dT_i}{dt} = \frac{\kappa(T_i)}{\delta_r^2}\left[\left(1 + \frac{1}{2\chi_i}\right)T_{i+1} - 2T_i + \left(1 - \frac{1}{2\chi_i}\right)T_{i-1}\right], \quad i = 1,\ldots,n, \tag{2.4}$$

*This PDE is not confined to wafers but is employed for various materials.

where the LHS follows by regarding the LHS of (2.1) as an ODE.

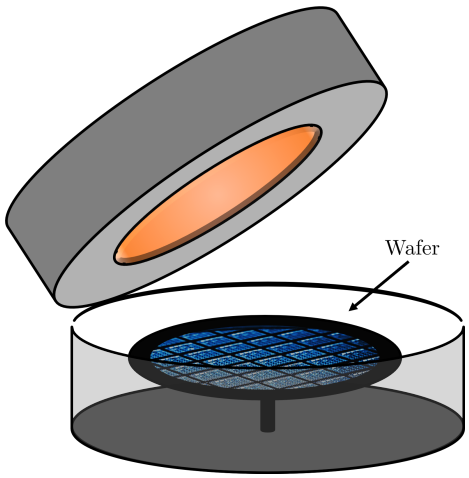

Figure 1. Diagram of the RTA process.

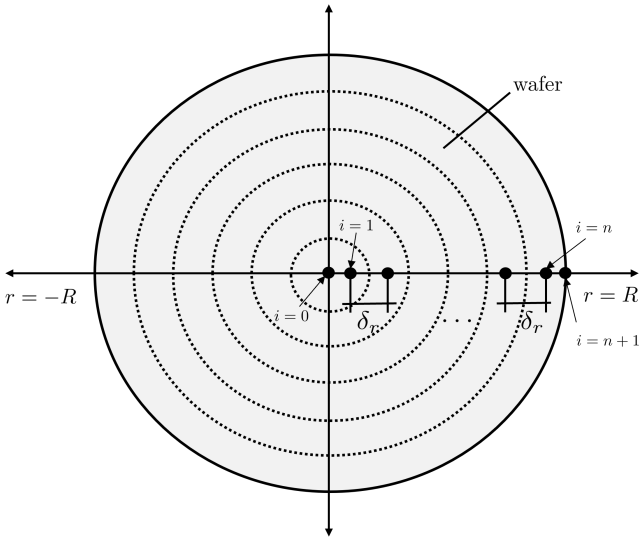

Figure 2. An equally distributed spatial grid used in discretization of the PDE in space.

With respect to solving (2.4), it should be required to consider the initial condition at the time instance $t = 0$ and the boundary conditions at non-uniformly distributed points $T_0 := T(0, t)$ and $T_{n+1} := T(R, t)$. In connection with this, the following Neumann boundary condition is taken in [11].

$$\left.\frac{\partial T(r,t)}{\partial r}\right|_{r=R} = 0. \tag{2.5}$$

This together with employing the forward difference equation given by

$$\frac{\partial T(R,t)}{\partial r} \approx \frac{T_{n+1} - T_n}{\delta_r} = 0 \tag{2.6}$$

leads to the following boundary condition at T_{n+1}.

$$T_{n+1} = T_n. \tag{2.7}$$

Similarly, the boundary condition at the center of the wafer can also be given by [11]

$$T_0 = T_1. \tag{2.8}$$

In addition to the above conditions, we next consider the case such that a lamp is given. Assume that the density function D with respect to a light absorption is assumed to follow a Gaussian distribution in terms of the distance s with the zero mean and the standard deviation σ_l. In other words, the density function is described by

$$D(s) = \frac{1}{\sigma_l \sqrt{2\pi}} \exp\left(-\frac{1}{2}\frac{s^2}{\sigma_l^2}\right). \tag{2.9}$$

To align with the central difference approximation given by (2.4), the density function of (2.9) is reinterpreted at the distance $s = \delta_r$ as follows.

$$D_k = D(k\delta_r), \quad k = 0, 1, \cdots, \infty. \tag{2.10}$$

Here, it should be remarked that the intensity factors $D_0, D_1, \ldots$ are assumed to be scaled such that

$$\sum_{k=0}^{\infty} D_k = 1 \tag{2.11}$$

instead of taking $\int_0^{\infty} D(s)ds = 1$ with respect to (2.9). In this line, a lamp located in the ring i transfers heat to the ring j with the corresponding intensity factor $D_{|i-j|}$.

Next, the temperature dynamics of the ring i with its area $S_i = (2i-1)(\delta_r)^2\pi$ can be described by

$$\frac{dT_i}{dt} = \frac{P_i}{\rho h c_p(T_i) S_i}, \tag{2.12}$$

where P_i denotes the total amount of power absorbed in the ring i and h is thickness of the wafer. Let N_u ($\mu = 1, \ldots, n$) be the number of lamps located in the ring μ. Then, the total power P_i can be computed by

$$P_i = \eta \sum_{\mu=1}^{n} \sum_{\nu=1}^{2n} N_\mu P_{\mu,e} D_{\nu-1} \frac{S_{i,\mu,\nu}}{\sum_{\tau=1}^{n} S_{\tau,\mu,\nu}}, \tag{2.13}$$

where $\eta \in [0, 1]$ is the efficiency factor, and $P_{\mu,e}$ is the electrical input power per lamp in the ring μ. $S_{i,\mu,\nu}$ denotes the overlapping area between the ring i centered on the wafer and the ring ν centered on the lamp as shown in Figure 3. Here, μ represents the ring centered on the wafer, where the lamp is positioned. Substituting (2.13) into (2.12) allows us to obtain the following differential equation describing the temperature dynamics of the ring i with respect to light absorption.

$$\frac{dT_i}{dt} = \frac{\eta}{\rho h c_p(T_i) S_i} \sum_{\mu=1}^{n} \sum_{\nu=1}^{2n} N_\mu P_{\mu,e} D_{\nu-1} \frac{S_{i,\mu\nu}}{\sum_{\tau=1}^{n} S_{\tau,\mu,\nu}}. \tag{2.14}$$

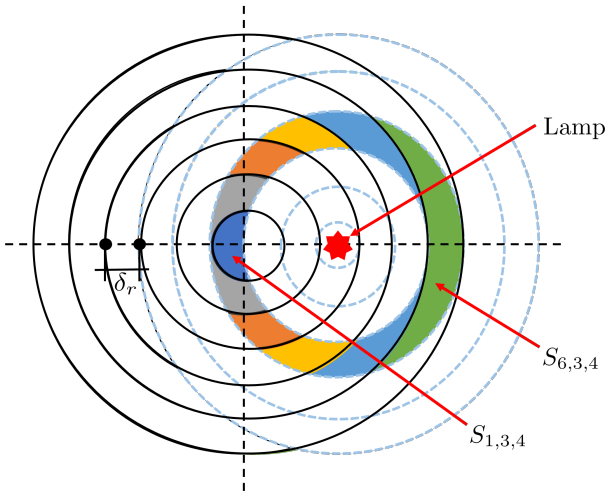

Figure 3. Illustration of the absorption of light emitted by a lamp to different rings.

The remaining task to derive complete temperature dynamics is to consider heat losses due to temperature differences relative to ambient conditions. Such heat losses on the wafer are primarily caused by thermal convections and radiations. Assuming that a constant ambient temperature, i.e., $T_e = 300$, around the wafer surface, the heat loss due to a convection, is given by

$$\frac{dT_i}{dt} = \frac{\alpha_i}{\rho h c_p(T_i)}(T_e - T_i), \tag{2.15}$$

where α_i denotes the heat transfer coefficient at the radius r_i. The heat loss due to a radiation is given by the Stefan-Boltzmann law, i.e.,

$$\frac{dT_i}{dt} = -2\frac{\epsilon\sigma_{sb}}{\rho h c_p(T_i)}T_i^4, \tag{2.16}$$

where ϵ is the total emissivity of the material, σ_{sb} is the Stefan-Boltzmann constant, and the factor 2 is for dealing with heat losses from both upper and lower surfaces of the wafer.

Combining the heat equation (2.4), the boundary conditions (2.7) and (2.8), the light absorption (2.14), and the heat losses (2.15) and (2.16) leads to the overall heat transfer process described by

$$\dot{x} = f(x,u) = A_1(x)x - \epsilon A_2(x)\begin{bmatrix} x_1^4 \\ x_2^4 \\ \vdots \\ x_n^4 \end{bmatrix} + B(x)u, \tag{2.17}$$

where $x = \begin{bmatrix} T_1 & T_2 & \cdots & T_n \end{bmatrix}^T \in \mathbb{R}^n$ is the state vector, $u = \begin{bmatrix} P_{1,e} & P_{2,e} & \cdots & P_{m,e} & T_e \end{bmatrix}^T =: \begin{bmatrix} u_c^T & T_e \end{bmatrix}^T \in \mathbb{R}^{m+1}$ is the control input, where u_c denotes the changeable input, and $m := N_1 + N_2 + \cdots + N_n$ is the

total number of lamps, with the matrices given by

$$A_1(x) = \operatorname{diag}\left(\frac{\kappa(x_i)}{(\delta_r)^2}\right)\begin{bmatrix} \frac{-1-2\chi_1}{2\chi_1} & \frac{1+2\chi_1}{2\chi_1} & 0 & \cdots & \cdots & 0 \\ \frac{-1+2\chi_2}{2\chi_2} & -2 & \frac{1+2\chi_2}{2\chi_2} & 0 & \cdots & 0 \\ & \ddots & \ddots & \ddots & & \\ 0 & \cdots & 0 & \frac{-1+2\chi_{n-1}}{2\chi_{n-1}} & -2 & \frac{1+2\chi_{n-1}}{2\chi_{n-1}} \\ 0 & \cdots & \cdots & 0 & \frac{-1+2\chi_n}{2\chi_n} & \frac{1-2\chi_n}{2\chi_n} \end{bmatrix} - \operatorname{diag}\left(\frac{\alpha_i}{\rho h c_p(x_i)}\right), \tag{2.18}$$

$$A_2(x) = \operatorname{diag}\left(\frac{2\sigma_{sb}}{\rho h c_p(x_i)}\right), \tag{2.19}$$

$$B(x) = \frac{1}{\rho h}\begin{bmatrix} \frac{\eta N_1}{c_p(x_1)S_1}\sum_{\nu=1}^{2n} D_{\nu-1}\frac{S_{1,1,\nu}}{\sum_{\tau=1}^{n} S_{\tau,1,\nu}} & \cdots & \frac{\eta N_n}{c_p(x_1)S_1}\sum_{\nu=1}^{2n} D_{\nu-1}\frac{S_{1,n,\nu}}{\sum_{\tau=1}^{n} S_{\tau,n,\nu}} & \frac{\alpha_1}{c_p(x_1)} \\ \frac{\eta N_1}{c_p(x_2)S_2}\sum_{\nu=1}^{2n} D_{\nu-1}\frac{S_{2,1,\nu}}{\sum_{\tau=1}^{n} S_{\tau,1,\nu}} & \cdots & \frac{\eta N_n}{c_p(x_2)S_2}\sum_{\nu=1}^{2n} D_{\nu-1}\frac{S_{2,n,\nu}}{\sum_{\tau=1}^{n} S_{\tau,n,\nu}} & \frac{\alpha_2}{c_p(x_2)} \\ \vdots & \cdots & \vdots & \vdots \\ \frac{\eta N_1}{c_p(x_n)S_n}\sum_{\nu=1}^{2n} D_{\nu-1}\frac{S_{n,1,\nu}}{\sum_{\tau=1}^{n} S_{\tau,1,\nu}} & \cdots & \frac{\eta N_n}{c_p(x_n)S_n}\sum_{\nu=1}^{2n} D_{\nu-1}\frac{S_{n,n,\nu}}{\sum_{\tau=1}^{n} S_{\tau,n,\nu}} & \frac{\alpha_n}{c_p(x_n)} \end{bmatrix} Z, \tag{2.20}$$

$$Z = \begin{bmatrix} 1 & \cdots & 1 & & & & 0 \\ & & & 0 & & & \\ & & & & 1 & \cdots & 1 \\ & & & & & \vdots & \\ 0 & & & & & & 1 \end{bmatrix} \in \mathbb{R}^{(n+1)\times(m+1)}. \tag{2.21}$$

Here, note that the ith row with $i = 1$ (i.e., the first row) of Z is given by

$$\begin{bmatrix} 1 & \cdots & 1 & 0 & \cdots & 0 \end{bmatrix}, \tag{2.22}$$

where the number of ones is equal to N_1 and means the spatial elements of the first region. For $i = 2, \ldots, n$, the ith row of Z is given by

$$\begin{bmatrix} 0 & \cdots & 0 & 1 & \cdots & 1 & 0 & \cdots & 0 \end{bmatrix}, \tag{2.23}$$

where the one occurs from the $(N_1 + \cdots + N_{i-1} + 1)$th entry to the $(N_1 + \cdots + N_i)$th entry. The ith row with $i = n + 1$ (i.e., the last row) of Z is given by

$$\begin{bmatrix} 0 & \cdots & 0 & 1 \end{bmatrix}, \tag{2.24}$$

which corresponds to the ambient temperature component. The details of the parameters are also presented in Table 2.

Table 2. Parameters of the heat transfer model.

Parameter	Description	Unit
ρ	Density	kg/m^3
$\lambda_c(T)$	Heat conductivity	W/m·K
$c_p(T)$	Heat capacity	J/kg·K
h	Material thickness	m
η	Efficiency factor	–
ϵ	Total emissivity	–
α_i	Heat transfer coefficient	W/m^2·K
σ_{sb}	Stefan–Boltzmann constant	W/m^2·K^4

3. Main results

This section develops a robust stability condition and a robust controller synthesis for heat transfer systems with an RTA process. To put it another way, the main objective is to provide a computationally efficient method for achieving the RTA performance of nonlinear heat transfer systems introduced in the preceding section.

3.1. New modeling of heat transfer systems

Even though we derive the state-space based representation of heat transfer systems as in (2.17), it is still nontrivial to develop direct and intuitive methods of analysis and controller synthesis due to their parameter-varying nonlinear characteristics. To solve this difficulty, the local linearization in terms of the Taylor series expansion around the room temperature $(x^*, u^*) = \left(300 \cdot 1_n, \begin{bmatrix} 0 & \cdots & 0 & T_e \end{bmatrix}^T\right)$ derives

$$\dot{x} = f(x,u) =: \begin{bmatrix} f_1 \\ f_2 \\ \vdots \\ f_n \end{bmatrix} = f(x^*,u^*) + \left.\frac{\partial f}{\partial x}\right|_{(x^*,u^*)} (x - x^*) + \left.\frac{\partial f}{\partial u}\right|_{(x^*,u^*)} (u - u^*) + \frac{1}{2}\begin{bmatrix} (x-x^*)^T & (u-u^*)^T \end{bmatrix} \times_2 H_f(\zeta) \times_3 \begin{bmatrix} x - x^* \\ u - u^* \end{bmatrix}, \tag{3.1}$$

where $H_f(\zeta) \in \mathbb{R}^{n\times(n+m+1)\times(n+m+1)}$ denotes the Hessian tensor evaluated at an intermediate point $\zeta \in \mathcal{D}$, with the domain $\mathcal{D}$ defined as the physical bounds on the state and control input, i.e.,

$$\mathcal{D} := \left\{ \begin{bmatrix} x^T & u^T \end{bmatrix}^T \in \mathbb{R}^{n+m+1} \mid x_i \in [x_{\min}, x_{\max}],\ u_j \in [u_{\min}, u_{\max}],\ \forall i = 1,\ldots,n;\ j = 1,\ldots,m+1 \right\}. \tag{3.2}$$

To simplify the notations, we define the linearization terms as follows:

$$\bar{f} := f(x^*,u^*) \in \mathbb{R}^n, \quad \bar{A} := \left.\frac{\partial f}{\partial x}\right|_{(x^*,u^*)} \in \mathbb{R}^{n\times n}, \quad \bar{B} := \left.\frac{\partial f}{\partial u}\right|_{(x^*,u^*)} \in \mathbb{R}^{n\times(m+1)}. \tag{3.3}$$

In a compatible fashion to $u = \begin{bmatrix} u_c^T & T_e^T \end{bmatrix}^T$, the input matrix $\bar{B}$ can also be decomposed into $\bar{B} = \begin{bmatrix} \bar{B}_1 & \bar{B}_2 \end{bmatrix}$ with $\bar{B}_1 \in \mathbb{R}^{n\times m}$ and $\bar{B}_2 \in \mathbb{R}^{n\times 1}$. Letting $\bar{x} := x - x^*$ and $\bar{u} := u - u^* = \begin{bmatrix} u_c^T & 0 \end{bmatrix}^T$ in (3.1) leads to the linear system given by

$$\dot{\bar{x}} = \bar{A}\bar{x} + \bar{B}\bar{u} + \bar{f} + \frac{1}{2}\begin{bmatrix} \bar{x}^T & \bar{u}^T \end{bmatrix} \times_2 H_f(\zeta) \times_3 \begin{bmatrix} \bar{x} \\ \bar{u} \end{bmatrix} = \bar{A}\bar{x} + \bar{B}_1 u_c + \bar{f} + \frac{1}{2}\begin{bmatrix} \bar{x}^T & \bar{u}^T \end{bmatrix} \times_2 H_f(\zeta) \times_3 \begin{bmatrix} \bar{x} \\ \bar{u} \end{bmatrix}, \quad (3.4)$$

where we use the property $dx^*/dt = 0$. We next take $\mathbf{H}(\zeta, \bar{x}, \bar{u})$ by

$$\mathbf{H}(\zeta, \bar{x}, \bar{u}) := \begin{bmatrix} \bar{x}^T & \bar{u}^T \end{bmatrix} \times_2 H_f(\zeta) \times_3 \begin{bmatrix} \bar{x} \\ \bar{u} \end{bmatrix}. \quad (3.5)$$

Then, (3.4) admits the representation

$$\dot{\bar{x}} = \bar{A}\bar{x} + \bar{B}_1 u_c + \bar{f} + \frac{1}{2}\mathbf{H}(\zeta, \bar{x}, \bar{u}) =: \bar{A}\bar{x} + \bar{B}_1 u_c + \bar{f} + w_{\mathrm{i}}, \quad (3.6)$$

where

$$w_{\mathrm{i}} := \frac{1}{2}\mathbf{H}(\zeta, \bar{x}, \bar{u}). \quad (3.7)$$

Here, $\bar{f}$ corresponds to the constant bias occurring from the linearization offset, while w_{i} is associated with higher-order nonlinear residuals and the subscript 'i' stands for the interconnected term. The following subsections are devoted to developing a robust stability condition for w_{i} and a robust tracking controller in the presence of $\bar{f}$ and w_{i}.

Remark 1. *Even though the proposed linearization is considered at the fixed point* $(x^*, u^*) = \left(300 \cdot 1_n, \begin{bmatrix} 0 & \cdots & 0 & T_e \end{bmatrix}^T\right)$*, this does not affect the essentials of the arguments. This is because the representation given by* (3.6) *and* (3.7) *and their associated properties (such as boundness, constant bias, and so on) do not depend on the operating point* (x^*, u^*)*. Thus, the arguments discussed in the following subsections can be equivalently established, regardless of the choice of* (x^*, u^*)*.*

3.2. L_1 robust stability analysis

As a preliminary step to developing a robust stability condition, we first take z_{i} by

$$z_{\mathrm{i}} := \begin{bmatrix} \bar{x}^T & u_c^T \end{bmatrix}^T, \quad (3.8)$$

where the subscript 'i' stands for the interconnected term. Next, we define the generalized plant P as

$$P : \begin{cases} \dot{\bar{x}} &= \bar{A}\bar{x} + \bar{B}_1 u_c + \bar{f} + w_{\mathrm{i}} \\ z_{\mathrm{i}} &= \begin{bmatrix} \bar{x} \\ u_c \end{bmatrix} \\ y &= \bar{x} \end{cases}, \quad (3.9)$$

where the measurement output is given by $y := \bar{x}$. Then, the heat transfer system with the RTA process given by (3.6) can be depicted as Figure 4. As clarified from this figure, the stability of the

overall system depends on the perturbation term $w_{\rm i}$ due to its inclusion in the feedback loop, while the feedforward term $\bar{f}$ does not affect the stability. With respect to this, we deal with the robust stability analysis associated with $w_{\rm i}$.

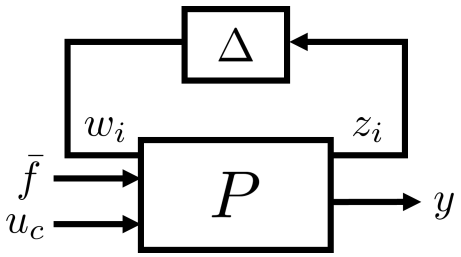

Figure 4. Interconnected system Σ.

To do this, we note from (3.5) and $\bar{u} = \begin{bmatrix} u_c^T & 0 \end{bmatrix}^T$ that

$$\mathbf{H}(\zeta, \bar{x}, \bar{u}) = \mathbf{H}_0(\zeta, \bar{x}, u_c) = \bar{x}^T \frac{\partial^2 f(\zeta)}{\partial x^2} \bar{x} + u_c^T \frac{\partial^2 f(\zeta)}{\partial u \partial x} \bar{x} + \bar{x}^T \frac{\partial^2 f(\zeta)}{\partial x \partial u} u_c + u_c^T \frac{\partial^2 f(\zeta)}{\partial u^2} u_c, \tag{3.10}$$

and this admits the quadratic form given by

$$\mathbf{H}_0(\zeta, \bar{x}, u_c) = z_{\rm i}^T \begin{bmatrix} \dfrac{\partial^2 f(\zeta)}{\partial x^2} & \dfrac{\partial^2 f(\zeta)}{\partial x \partial u} \\ \dfrac{\partial^2 f(\zeta)}{\partial u \partial x} & \dfrac{\partial^2 f(\zeta)}{\partial u^2} \end{bmatrix} z_{\rm i} =: \Delta(\zeta, z_{\rm i}) z_{\rm i}. \tag{3.11}$$

In other words, this $\Delta(\zeta, z_{\rm i})$ (defined as (3.11)) corresponds to the model uncertainty occurring from the linearization of (2.17). With this Δ in mind, the robust stability notion in this subsection is based on the small-gain theorem [18], in which $\Delta(\zeta, z_{\rm i})$ is required to be bounded in terms of an operator norm. With respect to this, we note from (3.2) that the domain $\mathcal{D}$ associated with $(\zeta, \bar{x}, u_c)$ is compact (i.e., bounded and closed). This together with the fact that the second-order partial derivative in (3.11) is continuous in ζ implies that $\Delta(\zeta, z_{\rm i})$ defined in (3.11) is uniformly continuous and bounded over $\mathcal{D}$. Thus, there should exist a constant γ (> 0) such that

$$\|\Delta(\zeta, z_{\rm i})\|_\infty \leq \gamma, \quad \forall \zeta \in \mathcal{D},\ \forall z_{\rm i} \in \mathcal{D}_0, \tag{3.12}$$

where

$$\mathcal{D}_0 := \Big\{ \begin{bmatrix} \bar{x}^T & u_c^T \end{bmatrix}^T \mid \bar{x}_i \in [\max\{x_{\min} - x^*, 0\}, \max\{x_{\max} - x^*, 0\}], \quad u_{cj} \in [u_{\min}, u_{\max}], \\ \forall i = 1, \ldots, n;\ j = 1, \ldots, m \Big\}. \tag{3.13}$$

The remaining task to employ the small-gain theorem [18] is to derive an associated subsystem of P counterpart to Δ. From (3.9), such a subsystem is denoted by $P_{\rm ii}$ and is defined as

$$P_{\rm ii} : \begin{cases} \dot{\bar{x}} &= \bar{A}\bar{x} + \bar{B}_1 u_c + w_{\rm i} \\ z_{\rm i} &= \begin{bmatrix} \bar{x} \\ u_c \end{bmatrix} \end{cases}. \tag{3.14}$$

Assume that a linear stabilizing controller $K : \bar{x} \mapsto u_c$ for P_{ii} is given (and the details for the design of the overall control architecture will be provided in Subsection 3.3). Then, let us denote the closed-loop system consisting of P_{ii} and the stabilizing controller K by Σ_{ii}. With employing the L_∞-induced norm of Σ_{ii} from w_{i} to z_{i}, which is denoted by $\|\Sigma_{\mathrm{ii}}\|_\infty$, we can obtain the following L_1 robust stability condition.

Theorem 1. *The interconnected system Σ in Figure 4 is robustly stable for the model uncertainty Δ described by* (3.12) *if*

$$\|\Sigma_{\mathrm{ii}}\|_\infty \cdot \gamma < 1. \tag{3.15}$$

This theorem clearly constructs a robust stability condition for uncertain heat transfer systems. Furthermore, the fact that the L_∞-induced norm can be computed within an arbitrary degree of accuracy by using the arguments in [12, 16] obviously establishes the applicability of Theorem 1.

Remark 2. *With respect to a computational efficiency of Theorem 1, it might be required to consider the case of higher-dimensional systems. When one could not obtain $\|\Sigma_{\mathrm{ii}}\|_\infty$ in a desired level by using the arguments [12, 16], it would be better to take the assertions in [19], because the latter study leads to quantitatively improved computations of the L_∞-induced norm than the former studies under the same computation parameter.*

Remark 3. *Even though several physical parameters (such as the efficiency factor η, the radiation loss coefficient ε, and so on) are assumed to be known in deriving the nominal model, this assumption does not affect the essentials of the arguments, especially for the L_1 robust stability condition in Theorem 1. More precisely, variations in these parameters can be naturally regarded as parts of the modeling uncertainty Δ and the nonlinear residual w_{i}, and they affect only the value of γ in* (3.12)*, but the L_1 robust stability condition* (3.15) *is still established.*

3.3. 2-DoF robust LQI control

This section provides a 2-DoF robust LQI control, by which the effects of w_{i} and $\bar{f}$ on the associated RTA performance can be reduced.

To this end, we first assume that no model uncertainty exists, and, thus, (3.6) is simplified by

$$\dot{\bar{x}} = \bar{A}\bar{x} + \bar{B}_1 u_c. \tag{3.16}$$

Here, note that the pair $(\bar{A}, \bar{B}_1)$ is assumed to be stabilizable and $(I, \bar{A})$ is detectable. On the other hand, the RTA process aims at achieving a constant temperature of heat transfer systems as soon as possible. In this sense, suppose that the constant reference $r \in \mathbb{R}^n$ is given. We further assume that $m = n$ and $\bar{B}_1 \in \mathbb{R}^{n\times n}$ is full-rank without loss of generality; note from [21] that the condition $m \geq n$ is required for general multivariable servo systems to ensure the zero steady-state error for all elements of $r \in \mathbb{R}^n$, and we take the mild assumption of $m = n$. On the basis of the internal model principle [20], it should be required to assume that

$$\mathrm{rank}\left(\begin{bmatrix} \bar{A} - \lambda I & \bar{B}_1 \\ I & 0 \end{bmatrix}\right) = 2n \tag{3.17}$$

for any eigenvalue $\lambda = 0$ of A_r, which generates the model of r, for achieving the zero steady-state error. In this problem, it is determined that $\lambda = 0$ in (3.17) since the step reference r is taken. If the system (3.16) arrives at the zero tracking error, then the steady-state of $(\bar{x}, u_c)$ is determined by

$$\begin{bmatrix} 0 \\ r \end{bmatrix} = \begin{bmatrix} \bar{A} & \bar{B}_1 \\ I & 0 \end{bmatrix} \begin{bmatrix} \bar{x}_\infty \\ u_{c,\infty} \end{bmatrix}, \tag{3.18}$$

where $\bar{x}_\infty$ and $u_{c,\infty}$ denote the steady-state values of $\bar{x}$ and u_c, respectively, and such a pair $(\bar{x}_\infty, u_{c,\infty})$ is uniformity obtained since $\begin{bmatrix} \bar{A} & \bar{B}_1 \\ I & 0 \end{bmatrix}$ is invertible. We next define the error variables $\tilde{x}$ and $\tilde{u}$ as

$$\tilde{x}(t) := \bar{x}_\infty - \bar{x}(t), \qquad \tilde{u}(t) := u_{c,\infty} - u_c(t). \tag{3.19}$$

Combining (3.16)–(3.19) yields the error system as follows:

$$\begin{cases} \dot{\tilde{x}} = \bar{A}\tilde{x} + \bar{B}_1\tilde{u}, \\ e = \tilde{x}. \end{cases} \tag{3.20}$$

On the basis of (3.20), the objective function is given by

$$J = \int_0^\infty \{e(t)^T Q e(t) + \tilde{u}^T(t) R \tilde{u}(t)\} dt, \tag{3.21}$$

with $Q \succ 0$ and $R \succ 0$. Then, the optimal control law minimizing J is given by [22]

$$\tilde{u}(t) = F_0 \tilde{x}(t), \tag{3.22}$$

where

$$F_0 := -R^{-1}\bar{B}_1^T P, \tag{3.23}$$

and P is the unique positive-definite solution to the algebraic Riccati equation described by

$$\bar{A}^T P + P\bar{A} - P\bar{B}_1 R^{-1}\bar{B}_1^T P + Q = 0. \tag{3.24}$$

Remark 4. *The existence and uniqueness of a solution to the algebraic Riccati equation of* (3.24) *are ensured by the fact that the pair* $(\bar{A}, \bar{B}_1)$ *is stabilizable and the pair* $(I_n, \bar{A})$ *is detectable as in [23].*

It immediately follows from (3.19) and (3.22) that

$$u_c(t) = u_{c,\infty} - \tilde{u}(t) = u_{c,\infty} - F_0\tilde{x}(t) = u_{c,\infty} - F_0(\bar{x}_\infty - \bar{x}(t)) = F_0\bar{x}(t) + H_0 r, \tag{3.25}$$

where the feedforward gain H_0 is defined as

$$H_0 := \begin{bmatrix} -F_0 & I \end{bmatrix} \begin{bmatrix} \bar{A} & \bar{B}_1 \\ I & 0 \end{bmatrix}^{-1} \begin{bmatrix} 0 \\ I \end{bmatrix}, \tag{3.26}$$

since we can see from (3.18) that

$$-F_0\bar{x}_\infty + u_{c,\infty} = \begin{bmatrix} -F_0 & I \end{bmatrix} \begin{bmatrix} \bar{x}_\infty \\ u_{c,\infty} \end{bmatrix} = \begin{bmatrix} -F_0 & I \end{bmatrix} \begin{bmatrix} \bar{A} & \bar{B}_1 \\ I & 0 \end{bmatrix}^{-1} \begin{bmatrix} 0 \\ I \end{bmatrix} r. \tag{3.27}$$

Then, substituting (3.25) into (3.16) leads to the closed-loop system given by

$$\dot{\bar{x}} = (\bar{A} + \bar{B}_1 F_0)\bar{x} + \bar{B}_1 H_0 r. \tag{3.28}$$

Here, $\bar{A} + \bar{B}_1 F_0$ is Hurwitz stable, and, thus, there exists the inverse $(\bar{A} + \bar{B}_1 F_0)^{-1}$. The scheme of (3.25) is called a 2-DoF LQ control throughout the paper, since it consists of the feedback term $F_0\bar{x}(t)$ and the feedforward term $H_0 r$.

To clarify that $\bar{x} \to r$ as $t \to \infty$, from the point of view of (3.28) once again (although it is already ensured by the boundness of J in (3.21)), we note that

$$\begin{bmatrix} (\bar{A} + \bar{B}_1 F_0)^{-1} & 0 \\ 0 & I \end{bmatrix} \begin{bmatrix} \bar{A} & \bar{B}_1 \\ I & 0 \end{bmatrix} \begin{bmatrix} I & 0 \\ F_0 & I \end{bmatrix} \begin{bmatrix} I & -(\bar{A} + \bar{B}_1 F_0)^{-1}\bar{B}_1 \\ 0 & I \end{bmatrix} = \begin{bmatrix} I & 0 \\ I & -(\bar{A} + \bar{B}_1 F_0)^{-1}\bar{B}_1 \end{bmatrix}. \tag{3.29}$$

This clearly implies that there exists the inverse $-((\bar{A} + \bar{B}_1 F_0)^{-1}\bar{B}_1)^{-1}$ since $\begin{bmatrix} \bar{A} & \bar{B}_1 \\ I & 0 \end{bmatrix}$ is invertible. We further obtain from (3.29) that

$$\begin{bmatrix} \bar{A} & \bar{B}_1 \\ I & 0 \end{bmatrix}^{-1} = \begin{bmatrix} I & 0 \\ F_0 & I \end{bmatrix} \begin{bmatrix} I & -(\bar{A} + \bar{B}_1 F_0)^{-1}\bar{B}_1 \\ 0 & I \end{bmatrix} \begin{bmatrix} (\bar{A} + \bar{B}_1 F_0)^{-1} & 0 \\ -((\bar{A} + \bar{B}_1 F_0)^{-1}\bar{B}_1)^{-1}(\bar{A} + \bar{B}_1 F_0)^{-1} & -((\bar{A} + \bar{B}_1 F_0)^{-1}\bar{B}_1)^{-1} \end{bmatrix}. \tag{3.30}$$

Substituting (3.30) into (3.26) leads to

$$H_0 = -((\bar{A} + \bar{B}_1 F_0)^{-1}\bar{B}_1)^{-1}. \tag{3.31}$$

Hence, applying the final value theorem to the transfer function from r to $\bar{x}$ associated with (3.28) implies that

$$\lim_{t\to\infty} \bar{x}(t) = \lim_{s\to 0}(sI - (\bar{A} + \bar{B}_1 F_0))^{-1}\bar{B}_1 H_0 r = r. \tag{3.32}$$

The aforementioned arguments are developed in the assumption that no model uncertainty exists. In connection with this, we next deal with a robust LQI control framework for reducing the effects of $w_{\rm i}$ and $\bar{f}$ on the tracking error e. To this end, we introduce the variable ξ defined as

$$\xi(t) := \int_0^t e(\tau)d\tau = \int_0^t (r - \bar{x}(\tau))d\tau. \tag{3.33}$$

This together with (3.28) leads to the augmented system described by

$$\begin{cases} \begin{bmatrix} \dot{\bar{x}} \\ \dot{\xi} \end{bmatrix} = \begin{bmatrix} \bar{A} + \bar{B}_1 F_0 & 0 \\ -I & 0 \end{bmatrix} \begin{bmatrix} \bar{x} \\ \xi \end{bmatrix} + \begin{bmatrix} \bar{B}_1 H_0 \\ I \end{bmatrix} r + \begin{bmatrix} \bar{B}_1 \\ 0 \end{bmatrix} v(t) \\ z = \begin{bmatrix} I & 0 \end{bmatrix} \begin{bmatrix} \bar{x} \\ \xi \end{bmatrix} \end{cases} \tag{3.34}$$

where v is an additional control input to reduce the effects of $w_{\rm i}$ and $\bar{f}$. For the case of $w_{\rm i} = 0$ and $\bar{f} = 0$, we can obtain that

$$\bar{x} = (\bar{A} + \bar{B}_1 F_0)^{-1}\dot{\bar{x}} - (\bar{A} + \bar{B}_1 F_0)^{-1}\bar{B}_1 H_0 r. \tag{3.35}$$

This together with $e(t) = r - \bar{x}(t)$ leads to

$$\begin{aligned} e(t) &= r - \bar{x}(t) \\ &= r - (\bar{A} + \bar{B}_1 F_0)^{-1} \dot{\bar{x}}(t) + (\bar{A} + \bar{B}_1 F_0)^{-1} \bar{B}_1 H_0 r \\ &= -(\bar{A} + \bar{B}_1 F_0)^{-1} \dot{\bar{x}}(t), \end{aligned} \tag{3.36}$$

where we employ the property of (3.31). Substituting (3.36) into (3.33) leads to

$$\xi(t) = \int_0^t e(\tau) d\tau + \xi(0) = -F_1 \bar{x}(t) + F_1 \bar{x}(0) + \xi(0), \tag{3.37}$$

where

$$F_1 := (\bar{A} + \bar{B}_1 F_0)^{-1}. \tag{3.38}$$

With respect to this, we define a virtual signal as

$$p(t) := F_1 \bar{x}(t) + \xi(t) - F_1 \bar{x}_0 - \xi_0, \tag{3.39}$$

and it is established that

$$p(t) = 0, \qquad \forall t \geq 0, \tag{3.40}$$

if $w_{\mathrm{i}} = 0$ and $\bar{f} = 0$. Otherwise, $p(t) \neq 0$ for some $t \geq 0$.

In this sense, we consider to take the additional control input by

$$v(t) = Gp(t) = G(F_1 \bar{x}(t) + \xi(t) - F_1 \bar{x}_0 - \xi_0) \tag{3.41}$$

to ensure that the homogeneous behavior corresponding to $p(t)$ is asymptotically stable. Substituting (3.41) into (3.34) derives the overall closed-loop system given by

$$\begin{cases} \begin{bmatrix} \dot{\bar{x}} \\ \dot{\xi} \end{bmatrix} = \begin{bmatrix} \bar{A} + \bar{B}_1(F_0 + GF_1) & \bar{B}_1 G \\ -I & 0 \end{bmatrix} \begin{bmatrix} \bar{x} \\ \xi \end{bmatrix} + \begin{bmatrix} \bar{B}_1 H_0 \\ I \end{bmatrix} r - \begin{bmatrix} \bar{B}_1 G \\ 0 \end{bmatrix} (F_1 \bar{x}(0) + \xi(0)), \\ z = \begin{bmatrix} I & 0 \end{bmatrix} \begin{bmatrix} \bar{x} \\ \xi \end{bmatrix}. \end{cases} \tag{3.42}$$

To achieve the desired behavior in a clearer fashion, we take the equivalent transformation as

$$\begin{bmatrix} \bar{x} \\ p \end{bmatrix} = \begin{bmatrix} I & 0 \\ F_1 & I \end{bmatrix} \begin{bmatrix} \bar{x} \\ \xi \end{bmatrix}, \tag{3.43}$$

by which we obtain that

$$\begin{cases} \begin{bmatrix} \dot{\bar{x}} \\ \dot{p} \end{bmatrix} = \begin{bmatrix} \bar{A} + \bar{B}_1 F_0 & \bar{B}_1 G \\ 0 & F_1 \bar{B}_1 G \end{bmatrix} \begin{bmatrix} \bar{x} \\ p \end{bmatrix} + \begin{bmatrix} \bar{B}_1 H_0 \\ 0 \end{bmatrix} r - \begin{bmatrix} \bar{B}_1 G \\ F_1 \bar{B}_1 G \end{bmatrix} (F_1 \bar{x}(0) + \xi(0)), \\ z = \begin{bmatrix} I & 0 \end{bmatrix} \begin{bmatrix} \bar{x} \\ p \end{bmatrix}. \end{cases} \tag{3.44}$$

Since the matrix $\bar{A} + \bar{B}_1 F_0$ is Hurwitz stable, the internal (i.e., asymptotic) stability of the above overall closed-loop system given by (3.44) is ensured if, and only if, the matrix $F_1 \bar{B}_1 G$ is also Hurwitz stable. This requirement is easily achieved by taking the gain $G \in \mathbb{R}^{m \times n}$ as the form of

$$G := (F_1 \bar{B}_1)^{-1} \Lambda, \tag{3.45}$$

for any Hurwitz stable matrix $\Lambda \in \mathbb{R}^{n \times n}$; a typical choice is $\Lambda = \mathrm{diag}(\lambda_1, \ldots, \lambda_n)$ for $\lambda_i < 0$ ($\forall i = 1, \ldots, n$).

Under this structure, the final control input is given by

$$u_c(t) = F_0 \bar{x}(t) + G p(t) + H_0 r, \tag{3.46}$$

where F_0 is the feedback gain, G is the integral gain, and H_0 is the feedforward gain defined as (3.23), (3.31), and (3.45), respectively. The scheme of (3.46) is called a 2-DoF robust LQI control throughout the paper, and the overall control architecture is shown in Figure 5. Furthermore, the design procedure of u_c in (3.46) can be summarized as shown in Figure 6.

Remark 5. *As clarified from Figure 5, the stabilizing controller mentioned in the above Theorem 1 is determined by the state-feedback form of $u_c = F_0 \bar{x}$. Thus, the L_1 robust stability condition in Theorem 1 would be verified by computing $\|\Sigma\|_\infty$, in which Σ_{ii} is obtained by connecting P_{ii} and F_0.*

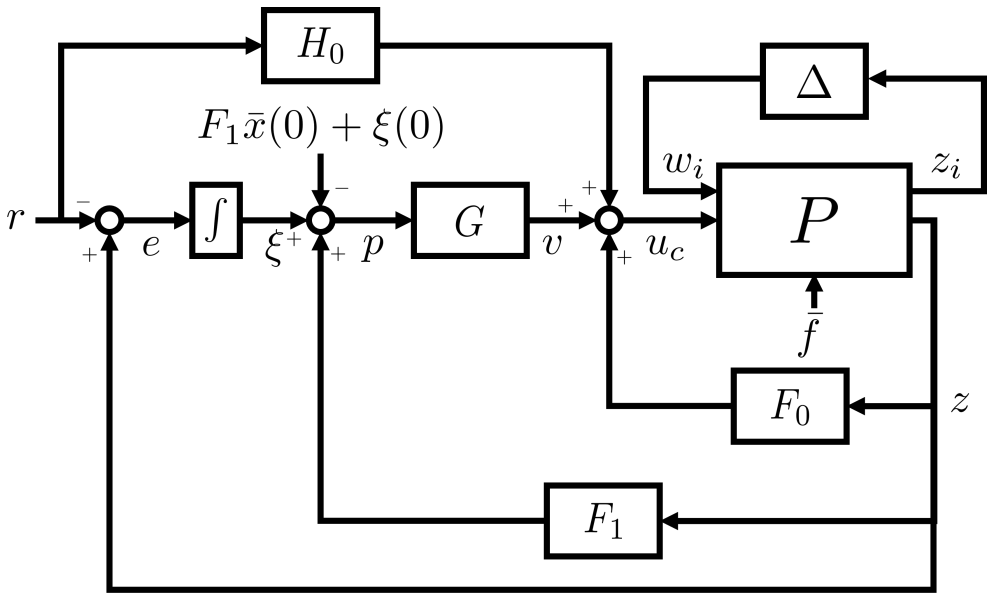

Figure 5. Proposed control structure with 2-DoF robust LQI.

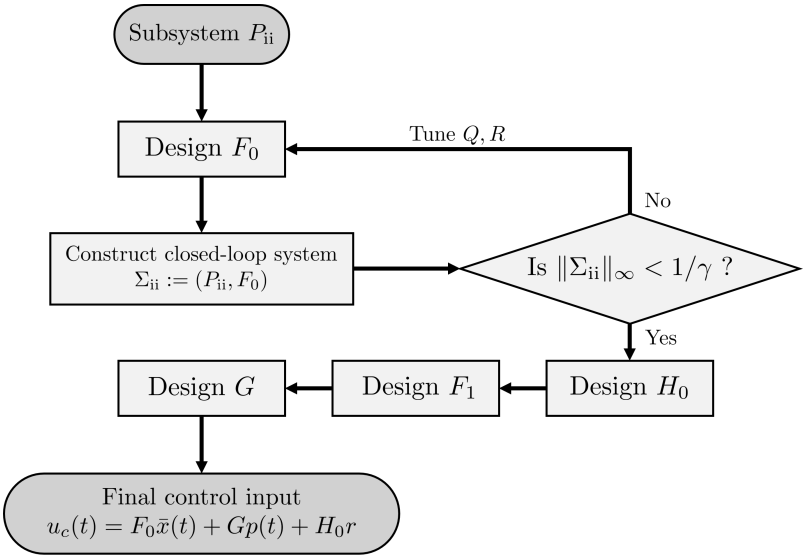

Figure 6. Schematic flow of the proposed control architecture.

4. Simulation results

This section provides some simulation results to demonstrate the proposed robust stability condition and robust controller synthesis for the nonlinear heat transfer system described by (2.17). The spatially discretized system consists of six concentric rings, and, thus, we obtain $x(t) \in \mathbb{R}^6$. The control input $u(t) \in \mathbb{R}^7$ includes six zone-specific heating commands and one ambient input. The six lamp channels are only activated (i.e., $m = 6$, $N_i = 1$ for all $i = 1, \cdots, 6$), while the ambient input is fixed at $T_e = 300K$. Hence, the actuator mapping matrix is given by

$$Z = I_7. \tag{4.1}$$

We further assume that the initial values of all the state variables are fixed at the ambient temperature, i.e.,

$$x(0) = 300 \cdot 1_6. \tag{4.2}$$

The reference trajectory is taken by a step signal [24, 25] as shown in Figure 7, i.e.,

$$r(t) = 800 \cdot 1_6, \quad \forall t \geq 0 \tag{4.3}$$

and we also consider the state and input constraints in (3.2) specified by

$$x_{\min} = 218, \qquad x_{\max} = 1687.15, \qquad u_{\min} = 0, \qquad u_{\max} = 200. \tag{4.4}$$

This constraint is constructed based on practical considerations: $x_{\min}$ reflects an extreme low-temperature condition by Joint Electron Device Engineering Council (JEDEC) standards [26], $x_{\max}$ is the melting point of silicon, $u_{\min}$ assumes no cooling capability, and $u_{\max}$ is an actuator limit. The other physical parameters used for the simulations are given in Table 3.

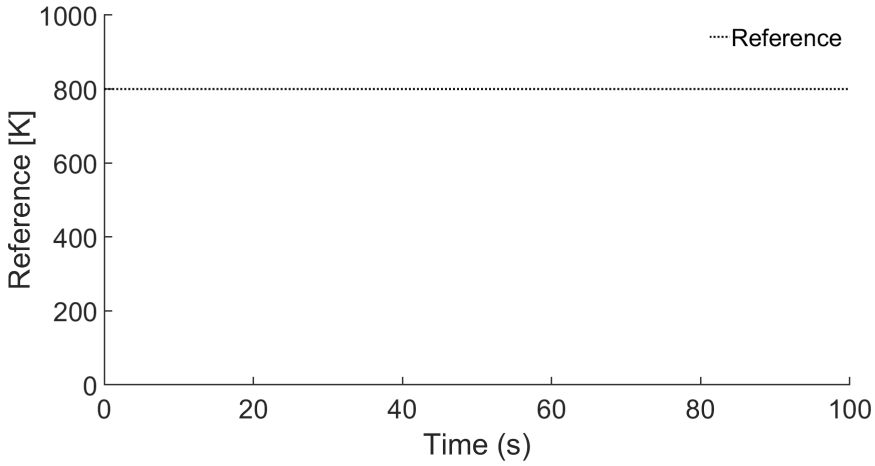

Figure 7. Reference trajectory (step input to $800K$ for all rings).

Table 3. Values of parameters for the heat transfer model.

Parameter	Description	Value	Unit
ρ	Density	2336	kg/m^3
$\lambda_c(T)$	Heat conductivity	$150\left(\frac{T}{300}\right)^{-1.3}$	W/m·K
$c_p(T)$	Heat capacity	$703 + \frac{255\left[\left(\frac{T}{300}\right)^{1.85} - 1\right]}{\left(\frac{T}{300}\right)^{1.85} + \frac{255}{703}}$	J/kg·K
h	Material thickness	775×10^{-6}	m
η	Efficiency factor	0.5	–
ϵ	Total emissivity	0.65	–
α_i	Heat transfer coefficient	1	W/m^2·K
σ_{sb}	Stefan–Boltzmann constant	5.6704×10^{-8}	W/m^2·K^4

By using these parameter values, we can obtain an upper bound on γ in (3.12) as 46.1292. Next, we consider the weighting matrices associated with (3.21) by

$$Q = qI_6, \qquad R = 50I_6, \qquad q \in \{500, 1500\}, \tag{4.5}$$

and the virtual-signal feedback gain in (3.45) is taken by

$$G = (F_1\bar{B}_1)^{-1}\Lambda, \qquad \Lambda = -50I_6. \tag{4.6}$$

Then, the control gains in (3.46) are given as follows:

$$F_0 = \begin{bmatrix} 0.1987 & 0.0264 & 0.0038 & 0.0003 & 0 & 0 \\ 0.0269 & 0.0685 & 0.0109 & 0.0017 & 0.0001 & 0 \\ 0.0038 & 0.0112 & 0.0404 & 0.0070 & 0.0011 & 0.0002 \\ 0.0004 & 0.0018 & 0.0072 & 0.0288 & 0.0052 & 0.0019 \\ 0 & 0.0003 & 0.0016 & 0.0056 & 0.0226 & 0.0096 \\ 0 & 0 & 0.0002 & 0.0017 & 0.0067 & 0.0453 \end{bmatrix}, \tag{4.7}$$

$$G = \begin{bmatrix} 0.0397 & -0.0316 & 0.0016 & 0.0009 & 0.0002 & -0.0001 \\ -0.0154 & 0.2413 & -0.0962 & 0.0028 & 0.0037 & -0.0001 \\ 0.0003 & -0.0622 & 0.6069 & -0.1919 & -0.0124 & 0.0070 \\ 0.0004 & 0.0013 & -0.1421 & 1.1360 & -0.3339 & -0.0015 \\ 0 & 0.0013 & 0.0027 & -0.2540 & 1.8487 & -0.3162 \\ 0 & -0.0001 & 0.0025 & 0.0070 & -0.3800 & 1.0616 \end{bmatrix} \times 10^5, \tag{4.8}$$

$$H_0 = \begin{bmatrix} 79.3592 & -31.5619 & 1.0744 & 0.4688 & 0.0810 & -0.0254 \\ -30.8958 & 241.3133 & -64.1347 & 1.3892 & 1.4910 & -0.0455 \\ 0.6950 & -62.1556 & 404.6003 & -95.9672 & -4.9467 & 2.3497 \\ 0.7446 & 1.2999 & -94.7650 & 567.9869 & -133.5681 & -0.5034 \\ -0.0531 & 1.2899 & 1.7925 & -126.9851 & 739.4873 & -105.3867 \\ -0.0155 & -0.1007 & 1.6900 & 3.5124 & -152.0016 & 353.8779 \end{bmatrix}. \tag{4.9}$$

For each q, the computation results for (3.15) are shown in Table 4. We can see from this table that the assertion $\|\Sigma_{ii}\|_\infty \cdot \gamma < 1$ is established for all q, and, thus, the resulting closed-loop systems satisfy the L_1 robust stability condition.

Table 4. Simulation results with respect to the L_1 robust stability.

q	500	1500
$\|\Sigma_{ii}\|_\infty \cdot \gamma$	0.0551	0.0552

Beyond the establishment of the L_1 robust stability, we next validate the effectiveness of taking the integral servo control given by (3.41) as well as the 2-DoF robust LQI control given by (3.46) through some comparative simulations. As mentioned in the preceding section, the integral term $Gp(t)$ is for reducing the effects of the offset $\bar{f}$ and the model uncertainty w_i, and, thus, it is expected that taking such a term could enhance not only the steady-state response but also the transient response in the presence of modeling errors.

To verify this expectation, we first compare the two scenarios: (i) 2-DoF LQ control (without the integral term (3.41), i.e., $G = 0$ in (3.46)) and (ii) 2-DoF LQI control (i.e., $G \neq 0$ in (3.46)), and the relevant simulation results are shown in Figure 8. We can observe from Figure 8(a,b) that the heat transfer system fails to track the reference signal for the case of 2-DoF LQ control, while the zero steady-state errors of the reference tracking are observed in Figure 8(c,d) for the case of 2-DoF robust LQI control. This clearly demonstrates the effectiveness of incorporating the integral control term $Gp(t)$ for reducing the effects of $\bar{f}$ and w_i on the reference tracking accuracy.

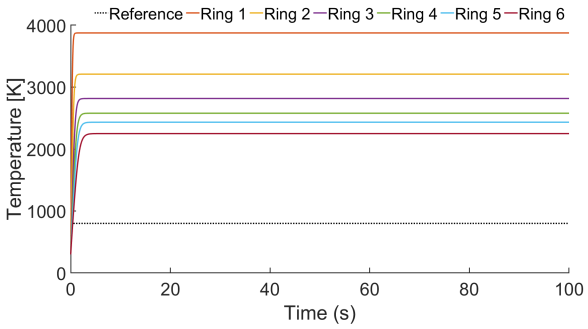

(a) 2-DoF LQ control with $q = 500$.

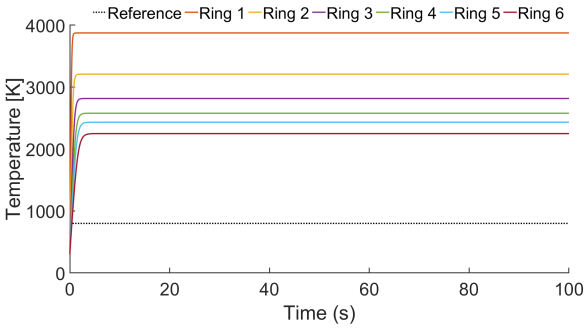

(b) 2-DoF LQ control with $q = 1500$.

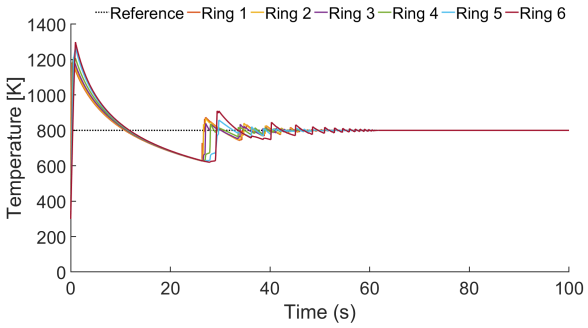

(c) 2-DoF robust LQI control with $q = 500$.

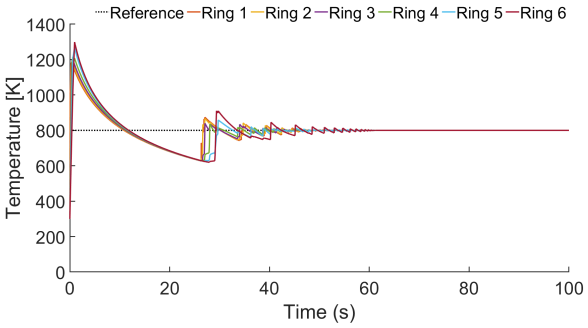

(d) 2-DoF robust LQI control with $q = 1500$.

Figure 8. Comparisons between 2-DoF LQ control and 2-DoF robust LQI control.

For verifying the practical effectiveness of the proposed 2-DoF robust LQI control in a quantitative fashion, we next conduct comparisons to the conventional observer-based method [11], in which an LQ controller and a Luenberger observer are taken for estimating and compensating the effects of modeling errors on the associated tracking accuracy. Because both the conventional and proposed methods have the common feature of employing the LQ control, we can take same parameters as in (4.5) for the former method and consider comparisons in a fair fashion. The simulations results for the conventional study [11] are shown in Figure 9.

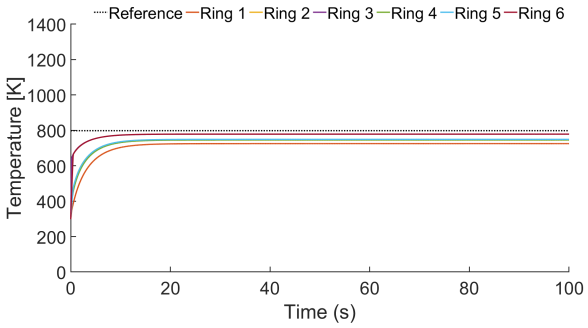

(a) Observer-based LQ control with $q = 500$.

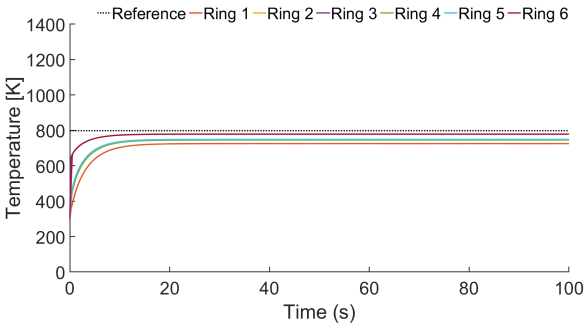

(b) Observer-based LQ control with $q = 1500$.

Figure 9. Simulation results for the conventional observer-based method [11].

It could be observed from Figure 9 that there exist nonzero steady-state errors of the reference tracking for the conventional observer-based LQ control [11]. For a more quantitative comparison between the conventional and proposed methods, we consider the two performance measures of the average steady-state error and the average root mean square (RMS) value of the input signal, which are denoted by $e_{\mathrm{ss,avg}}$ and $u_{\mathrm{rms,avg}}$ and defined, respectively, by

$$e_{\mathrm{ss,avg}} := \frac{1}{n}\sum_{i=1}^{n} |e_i(t_{\mathrm{end}})|, \tag{4.10}$$

$$u_{\mathrm{rms,avg}} := \frac{1}{m}\sum_{j=1}^{m} \sqrt{\frac{1}{T}\int_0^T u_j^2(t)dt}, \tag{4.11}$$

and the simulation results for these two performance measures are shown in Table 5.

Table 5. Comparisons between the proposed method and the conventional method [11].

q	Method	$e_{ss,avg}$	$u_{\mathrm{rms,avg}}$
500	Conventional method [11]	44.1441	164.9659
	Proposed method	0	16.0430
1500	Conventional method [11]	44.1252	164.9660
	Proposed method	0	16.0005

We can observe from Table 5 that the proposed method achieves obviously better reference tracking accuracy with a quite smaller energy of the control input than the conventional method under the same parameter (Q, R). This undoubtedly implies that the 2-DoF robust LQI control proposed in this paper is quite superior to the conventional observer-based LQ control developed in [11] for achieving the RTA process of heat transfer systems.

5. Conclusions

This study proposed a robust control framework tailored to spatially discretized heat transfer systems with focusing on the RTA process. We first discussed a description of heat transfer systems, and derived its tractable form in terms of a spatial discretization and the Taylor series expansion around the room temperature. Such a form allowed us to treat nonlinear heat transfer systems by an interconnection between a nonlinear model uncertainty and a linearized nominal system. Based on this interconnected representation, we established an L_1 robust stability condition, by which we can ensure the robust stability of heat transfer systems with modeling errors characterized in terms of the L_∞(-induced) norm. To achieve the zero steady-state error of the reference tracking for heat transfer systems in the presence of modeling errors, we next developed a 2-DoF robust LQI control method. In other words, this developed method was for reducing the effects of the modeling errors on the associated reference tracking accuracy. The effectiveness of the proposed 2-DoF LQI control was demonstrated through some simulations. Furthermore, we conducted some comparative simulations to the conventional observer-based LQ control [11] and showed that the proposed method is quite superior to the conventional method.

Finally, it would be worthwhile to note that an extension of the proposed method to large-scale or multi-zone thermal systems with time-delay and/or stochastic disturbances is also an important issue. In connection with this, employing a distributed or block-sparse controller [27] might lead to an accurate tracking accuracy for the case of higher spatial resolutions than those considered in this study. We also expect that taking predictor-based LQI schemes [28] or delay-dependent Lyapunov conditions [29] establishes robust stability conditions in the presence of time-delays. Furthermore, combining the mean-square stability [30] with the proposed framework might be used effectively for systems with stochastic disturbances. However, it is nontrivial to derive meaningful assertions on these directions, and it is left for an interesting future work.

Author contributions

Taewan Kim: original draft preparation, methodology, investigation, and formal analysis; Jung Hoon Kim: supervision, validation, manuscript-review, project administration, funding acquisition, and revisions; Jihyun Park: literature survey and preparation of additional figures. All authors have read and agreed to the published version of the manuscript.

Use of Generative-AI tools declaration

The authors declare they have not used Artificial Intelligence (AI) tools in the creation of this article.

Acknowledgments

This study was carried out with the support of 'R&D Program for Forest Science Technology (RS-2024-00403460)' provided by Korea Forest Service(Korea Forestry Promotion Institute).

Conflict of interest

The authors declare no conflicts of interest.

References

1. W. Yu, D. M. France, D. S. Smith, D. Singh, E. V. Timofeeva, J. L. Routbort, Heat transfer to a silicon carbide/water nanofluid, *Int. J. Heat Mass Transfer*, **52** (2009), 3606–3612. https://doi.org/10.1016/j.ijheatmasstransfer.2009.02.036
2. H. Guan, W. Xu, X. Li, H. Peng, Y. Feng, J. Zhang, et al., Implementation of photothermal annealing on ZnO electron transporting layer for high performance inverted polymer solar cells, *Mater. Lett.*, **163** (2016), 69–71. https://doi.org/10.1016/j.matlet.2015.10.016
3. M. Andresen, K. Ma, G. Buticchi, J. Falck, F. Blaabjerg, M. Liserre, Junction temperature control for more reliable power electronics, *IEEE Trans. Power Electron.*, **33** (2018), 765–776. https://doi.org/10.1109/TPEL.2017.2665697

4. J. Crank, P. Nicolson, A practical method for numerical evaluation of solutions of partial differential equations of the heat-conduction type, *Adv. Computat. Math.*, **6** (1996), 207–226. https://doi.org/10.1007/BF02127704
5. G. Comini, S. Del Guidice, R. W. Lewis, O. C. Zienkiewicz, Finite element solution of non-linear heat conduction problems with special reference to phase change, *Int. J. Numer. Methods Eng.*, **8** (1974), 613–624. https://doi.org/10.1002/nme.1620080314
6. M. N. Özişik, H. R. B. Orlande, M. J. Colaço, R. M. Cotta, *Finite difference methods in heat transfer*, 2 Eds., CRC press, 2017. https://doi.org/10.1201/9781315121475
7. R. Goldstein, W. E. Ibele, S. V. Patankar, T. W. Simon, T. H. Kuehn, P. J. Strykowski, et al., Heat transfer–A review of 2003 literature, *Int. J. Heat Mass Transfer*, **49** (2006), 451–534. https://doi.org/10.1016/j.ijheatmasstransfer.2005.11.001
8. W. K. Liu, S. Li, H. S. Park, Eighty years of the finite element method: birth, evolution, and future, *Arch. Comput. Method Eng.*, **29** (2022), 4431–4453. https://doi.org/10.1007/s11831-022-09740-9
9. D. Edouard, H. Hammouri, X. G. Zhou, Control of a reverse flow reactor for VOC combustion, *Chem. Eng. Sci.*, **60** (2005), 1661–1672. https://doi.org/10.1016/j.ces.2004.10.020
10. S. K. Al-Dawery, A. M. Alrahawi, K. M. Al-Zobai, Dynamic modeling and control of plate heat exchanger, *Int. J. Heat Mass Transfer*, **55** (2012), 6873–6880. https://doi.org/10.1016/j.ijheatmasstransfer.2012.06.094
11. M. Kleindienst, M. Reichhartinger, M. Horn, F. Staudegger, Observer-based temperature control of an LED heated silicon wafer, *J. Process Control*, **70** (2018), 96–108. https://doi.org/10.1016/j.jprocont.2018.07.006
12. O. R. Kang, J. H. Kim, The l_∞-induced norm of multivariable discrete-time linear systems: upper and lower bounds with convergence rate analysis, *AIMS Math.*, **8** (2023), 29140–29157. https://doi.org/10.3934/math.20231492
13. T. Kim, J. H. Kim, A new optimal control approach to uncertain Euler-Lagrange equations: H_∞ disturbance estimator and generalized H_2 tracking controller, *AIMS Math.*, **9** (2024), 34466–34487. https://doi.org/10.3934/math.20241642
14. H. Y. Park, J. H. Kim, Model-free control approach to uncertain Euler-Lagrange equations with a Lyapunov-based L_∞-gain analysis, *AIMS Math.*, **8** (2023), 17666–17686. https://doi.org/10.3934/math.2023902
15. H. T. Choi, J. H. Kim, The L_1 controller synthesis for piecewise continuous nonlinear systems via set invariance principles, *Int. J. Robust Nonlinear Control*, **33** (2023), 8670–8692. https://doi.org/10.1002/rnc.6843
16. D. Kwak, J. H. Kim, T. Hagiwara, Generalized fast-hold approximation approach to sampled-data L_1 synthesis, *IFAC-PapersOnLine*, **56** (2023), 9818–9822. https://doi.org/10.1016/j.ifacol.2023.10.401
17. D. Kwak, J. H. Kim, T. Hagiwara, A new quasi-finite-rank approximation of compression operators on $L_\infty[0, H)$ with applications to sampled-data and time-delay systems: Piecewise linear kernel approximation approach, *J. Franklin Inst.*, **361** (2024), 107271. https://doi.org/10.1016/j.jfranklin.2024.107271

18. U. Mackenroth, *Robust control systems: theory and case studies*, Springer Science & Business Media, 2004. https://doi.org/10.1007/978-3-662-09775-5

19. D. Kwak, J. H. Kim, T. Hagiwara, Generalized framework for computing the L_∞-induced norm of sampled-data systems, *Appl. Math. Comput.*, **437** (2023), 127518. https://doi.org/10.1016/j.amc.2022.127518

20. B. A. Francis, W. M. Wonham, The internal model principle of control theory, *Automatica*, **12** (1976), 457–465. https://doi.org/10.1016/0005-1098(76)90006-6

21. S. Boyd, M. Hast, K. J. Åström, MIMO PID tuning via iterated LMI restriction, *Int. J. Robust Nonlinear Control*, **26** (2016), 1718–1731. https://doi.org/10.1002/rnc.3376

22. H. Kwakernaak, R. Sivan, *Linear optimal control systems*, New York: Wiley-interscience, 1972.

23. K. Zhou, J. C. Doyle, K. Glover, *Robust and optimal control*, 1 Ed., Prentice hall, 1995.

24. J. R. Prekodravac, D. P. Kepić, J. C. Colmenares, D. A. Giannakoudakis, S. P. Jovanović, A comprehensive review on selected graphene synthesis methods: from electrochemical exfoliation through rapid thermal annealing towards biomass pyrolysis, *J. Mater. Chem. C*, **9** (2021), 6722–6748. https://doi.org/10.1039/D1TC01316E

25. R. Katsumata, C. Senger, J. N. Pagaduan, Recent advances and emerging opportunities in rapid thermal annealing (RTA) of polymers, *Mol. Syst. Des. Eng.*, **8** (2023), 701–712. https://doi.org/10.1039/D2ME00283C

26. JEDEC Solid State Technology Association, *JESD22-A104E: Temperature cycling*, 2015.

27. L. Furieri, Y. Zheng, A. Papachristodoulou, M. Kamgarpour, Sparsity invariance for convex design of distributed controllers, *IEEE Trans. Control Netw. Syst.*, **7** (2020), 1836–1847. https://doi.org/10.1109/TCNS.2020.3002429

28. S. Hu, X. Ren, D. Zheng, Integral predictor based prescribed performance control for multi-motor driving servo systems, *J. Franklin Inst.*, **359** (2022), 8910–8932. https://doi.org/10.1016/j.jfranklin.2022.07.021

29. E. Fridman, U. Shaked, Delay-dependent stability and H_∞ control: constant and time-varying delays, *Int. J. Control*, **76** (2003), 48–60. https://doi.org/10.1080/0020717021000049151

30. S. P. Nandanoori, A. Diwadkar, U. Vaidya, Mean square stability analysis of stochastic continuous-time linear networked systems, *IEEE Trans. Autom. Control*, **63** (2018), 4323–4330. https://doi.org/10.1109/TAC.2018.2830882

AIMS Press